

Submitted to ApJ

Deep Radio, Optical, and Infrared Observations of SGR 1900+14

D. L. Kaplan, S. R. Kulkarni

Department of Astronomy, 105-24 California Institute of Technology, Pasadena, California 91125, USA

`dlk@astro.caltech.edu, srk@astro.caltech.edu`

D. A. Frail

National Radio Astronomy Observatory, Socorro, NM 87801, USA

`dfrail@nrao.edu`

and

M. H. van Kerkwijk

Sterrenkundig Instituut, Universiteit Utrecht, Postbus 80000, 3508 TA Utrecht, The Netherlands

`M.H.vanKerkwijk@phys.uu.nl`

ABSTRACT

We present *HST*/STIS, Keck *J*- and *K_s*-band, and VLA 332-MHz and 1400-MHz images of the region around the Soft γ -ray Repeater SGR 1900+14. No non-stellar sources were detected at the position of SGR 1900+14, giving 3σ limits of $S_{332\text{ MHz}} < 6$ mJy, $S_{1.4\text{ GHz}} < 1.5$ mJy, $m_{50\text{CCD}} \gtrsim 29.0$ mag, $J \gtrsim 22.8$ mag, $K_s \gtrsim 20.8$ mag (point sources), and $S_{332\text{ MHz}} < 6.1$ mJy arcmin $^{-2}$, $S_{1.4\text{ GHz}} < 6.2$ mJy arcmin $^{-2}$ (extended emission). Given the very high extinction, the STIS and *J*-band non-detections are not constraining, but the *K_s*-band limit rules out basic accretion disk models for SGR 1900+14, and is almost comparable in depth to the *K_s*-band detection for the anomalous X-ray pulsar 4U 0142+61. Finally, we report the detection in this field of three new candidate supernova remnants, SNRs G043.5+00.6, G042.0–00.1, and G041.5+00.4.

Subject headings: infrared: stars — pulsars: individual (SGR 1900+14) — radio: supernova remnants — stars: neutron — X-rays: stars

1. Introduction

Soft γ -ray Repeaters (SGRs; see Hurley 2000 for a recent observational review) are sources both of bursts of hard X-rays/ γ -rays and softer quiescent X-ray emission. They are generally thought to be young ($< 10^4$ yr) neutron stars with extremely strong magnetic fields, or magnetars (e.g. Duncan & Thompson 1992; Thompson & Duncan 1993). This belief has been motivated by their associations with young supernova remnants (SNRs; Evans et al. 1980; Kulkarni & Frail 1993; Vasisht et al. 1994; but see Gaensler et al. 2001), the energetics of their bursts (Paczyński 1992; Thompson & Duncan 1995), and the detection of X-ray pulsations with long (5–10 s) periods and large ($\sim 10^{-11}$ s s $^{-1}$) spin-down rates (e.g. Kouveliotou et al. 1999).

An alternate theory, first proposed (van Paradijs et al. 1995; Chatterjee, Hernquist, & Narayan 2000) for the emission from the related Anomalous X-ray Pulsars (AXPs; see Mereghetti 2000), and now for the SGRs as well (Marsden et al. 2000; Marsden et al. 2001; but see Duncan 2001), is accretion from a “fallback” disk of material produced during the supernova explosion onto a central neutron star. In this model, the neutron stars are spinning near the equilibrium period which is proportional to the dipole field strength. This model then explains the spin-down and period clustering of the AXPs. For a typical field strength of 10^{12} G, the resultant spin period is ~ 8 s.

To date, no persistent counterparts have been found for SGRs at optical/IR or radio wavelengths (e.g. Kaplan et al. 2001). It generally has been the case that when counterparts are identified at other wavelengths, especially optical or IR, there is considerable progress in our understanding of these objects. For example, the identification of an optical/IR counterpart of the AXP 4U 0142+61 (Hulleman, van Kerkwijk, & Kulkarni 2000) has posed the strongest challenge to accretion models. In view of this, it is important to press upon sensitive multi-wavelength observations of SGRs. Here we present optical, IR, and radio observations of the very accurately localized SGR 1900+14 (Frail, Kulkarni, & Bloom 1999; Hurley et al. 1999d).

1.1. SGR 1900+14

SGR 1900+14 had been a relatively innocuous and quiescent source until late 1998. It had been associated with a soft, persistent X-ray source (Hurley et al. 1996) and a SNR, G042.8+00.6 (Vasisht et al. 1994). On 1998 August 27, the spacecraft Konus detected an intense burst of γ -rays (Hurley et al. 1999a). Arrival-time localization (Hurley et al. 1999c) soon identified SGR 1900+14 as the source. Prompt radio observations detected

a fading, non-thermal source (Frail et al. 1999) coincident with the X-ray source (Hurley et al. 1999d), and timing of the X-ray emission revealed a 5.16-s pulsar (Hurley et al. 1999d) with magnetar-like spin-down (Kouveliotou et al. 1999). The radio source associated with the 1998 August 27 burst is located at $\alpha_{2000} = 19^{\text{h}}07^{\text{m}}14\text{s}.33$, $\delta_{2000} = +09^{\circ}19'20''.1$, with uncertainty $\pm 0''.15$ in each coordinate (Frail et al. 1999).

Searches for SGR 1900+14 at wavelengths other than X-ray and γ -ray have not detected any significant quiescent counterpart (Hurley et al. 1996; Lorimer & Xilouris 2000; Eikenberry & Dror 2000; Vrba et al. 2000). However, Lorimer & Xilouris (2000) did detect a young (10^{4-5} yr) radio pulsar (PSR J1907+0918) located in the vicinity¹ of both SGR 1900+14 and G042.8+00.6, suggesting that G042.8+00.6 could be associated with PSR J1907+0918 just as easily as with SGR 1900+14.

Vrba et al. (2000) have suggested that SGR 1900+14 is somehow related to a compact cluster found in its vicinity (about $12''$ away). A similar cluster has been identified near SGR 1806–20 (Fuchs et al. 1999). We note, though, that no such cluster is found in the vicinity of SGR 0526-66 in the *HST* images presented by Kaplan et al. (2001). Furthermore, SGR 1806–20 and SGR 1900+14 are found at low Galactic latitudes in the inner Galaxy and the chance coincidence probability with star clusters, the rare Luminous Blue Variables (LBVs) and SNRs is not negligible (e.g. Gaensler et al. 2001). Indeed, there is now some doubt about the association of SGR 1806–20 with the SNR G10.0–0.3 (Hurley et al. 1999b). Nonetheless, the presence of star clusters in the vicinity of SGR 1900+14 appears intriguing. Our radio maps are deeper than previous images (e.g. Vasisht et al. 1994) and we find no radio source or nebulae associated with this star cluster (see Figures 3–5).

For the X-ray properties of SGR 1900+14 in what follows, we use the power-law + blackbody fit to the second epoch (the one closer to normal quiescence) of the recent *Chandra* observations by Fox et al. (2001): $N_H = 2.3 \pm 1 \times 10^{21} \text{ cm}^{-2}$, power-law index $\Gamma = 1.9 \pm 0.3$, blackbody temperature $kT \approx 0.49 \pm 0.03 \text{ keV}$, and an un-absorbed 0.5–10 keV X-ray flux $f_X^U = 2.0 \times 10^{-11} \text{ erg s}^{-1} \text{ cm}^{-2}$ (also see Kouveliotou et al. 2001). This is consistent with the *ASCA* measurements of Hurley et al. (1999d). We adopt a distance $d = 5 \text{ kpc}$ (Hurley et al. 1999d), which is based on hydrogen absorption. The hydrogen column density implies a visual extinction $A_V = 12.8 \pm 0.8 \text{ mag}$, assuming $N_H = 1.79 \pm 0.03 \times 10^{21} A_V \text{ cm}^{-2}$ (Predehl & Schmitt 1995). These values differ significantly from those assumed for the star cluster ($d = 12\text{--}15 \text{ kpc}$, $A_V \approx 19.2 \text{ mag}$; Vrba et al. 1996), and this difference may make the case for associating SGR 1900+14 and the cluster less compelling.

¹PSR J1907+0918 is located at $\alpha = 19^{\text{h}}07^{\text{m}}22\text{s}.441$, $\delta = +09^{\circ}18'30''.76$, with uncertainty $\pm 0''.05$ in each coordinate (Lorimer & Xilouris 2000).

2. Observations

We have carried out a campaign at optical/IR and radio wavelengths to detect SGR 1900+14. The radio data can also determine the existence of a low surface-brightness nebula surrounding SGR 1900+14, and localize SGR 1900+14 relative to nearby SNRs. See Table 1 for a log of all the observations.

2.1. Optical

The optical data consist of 5 exposures taken by the Space Telescope Imaging Spectrograph (STIS) aboard the *Hubble Space Telescope (HST)*, totaling 5195 s. The data were taken in imaging mode using the clear (50CCD) filter, giving a bandpass centered at roughly 585.2 nm and a full-width at half-maximum (FWHM) of ≈ 400 nm. The first exposure had a duration of 30 s, and was used for astrometry (see below). The remaining exposures were ~ 1300 -s long and were dithered in the usual manner to improve resolution and mitigate the effects of CCD irregularities.

The reduction followed the standard procedure for STIS images. We followed the standard drizzling reduction procedure (Fruchter & Mutchler 1998) expanding the individual pixels by a factor of two. This drizzling changed the pixel scale from $0''.05$ pixel $^{-1}$ to $0''.025$ pixel $^{-1}$. Typical stellar sources had a FWHM of $0''.095$; see Figure 1.

For the astrometry, we selected from the USNO-A2.0 catalogue (Monet 1998) all 76 stars that overlapped with a 30-s R-band image taken on 28 August 1998 with the Low-Resolution Imaging Spectrograph (LRIS; Oke et al. 1995) on the Keck telescope. For the 54 stars that were not overexposed, we measured centroids and corrected for instrumental distortion using a bi-cubic function determined by J. Cohen (1997, private communication). We used these to solve for the zero-points in each coordinate, the plate scale, and the position angle on the sky. After rejecting 8 outliers (residual larger than $0''.8$), the root-mean-square residuals were $0''.29$ in each coordinate. This is somewhat larger than we found for other projects, but not atypical for relatively crowded Galactic fields on the Northern hemisphere. Given this, the astrometry is tied to the USNO-A2.0 system at the $0''.05$ level. The typical accuracy with which the USNO-A2.0 catalogue is on the International Celestial Reference Frame (ICRF) is about $0''.2$ (Deutsch 1999).

The astrometry was transferred to the STIS image using 43 stars close to the radio position, solving again for plate scale, rotation and zero-points. The rms residuals were $0''.02$ in each coordinate, giving an overall astrometric uncertainty of $0''.21$ in each coordinate. The 3- σ limiting magnitude, based on calibration using the photometric keywords in the image

header, is 29.0, or $f_{\nu,\min} = 10 \text{ nJy}^2$.

2.2. Infrared

The infrared data were taken with the Near Infrared Camera (NIRC; Matthews & Soifer 1994) mounted on the 10-m Keck I telescope. The observations had photometric conditions and very good seeing ($0''.35$ at K_s -band). The data were reduced with custom **IRAF** software. The images were dark subtracted, flat-fielded, and corrected for bad pixels and cosmic rays. We then made object masks, which were used to construct improved flat fields for a second round of reduction. The data were finally registered, shifted, and co-added; see Figure 2.

The astrometry was performed with 50 stars from the deep STIS image. This solution had errors of $\pm 0''.04$ (in each coordinate) relative to the STIS image, or again $\pm 0''.21$ relative to the ICRF. For photometric calibration we used the standard star SJ 9101 (Persson et al. 1998). The 3σ limiting magnitudes are $K_s \approx 20.8$ and $J \approx 22.8$, corresponding to $f_{\nu,K_s} \approx 3.1 \mu\text{Jy}$ and $f_{\nu,J} \approx 1.2 \mu\text{Jy}$, based on the calibration of Bessell, Castelli, & Plez (1998).

2.3. Radio

The 1.4-GHz data were taken at the Very Large Array (VLA) in its C and D configurations using the standard continuum mode, with 2×50 MHz bandwidth. The separate observations were calibrated independently, following the standard procedure in **AIPS**. The phase calibrator was JVAS J1925+2106, and the flux calibrator was 3C 48. The data were then self-calibrated and combined for imaging. The nominal beam size was $\approx 20''$, and the rms noise is $\approx 0.5 \text{ mJy beam}^{-1}$; see Figure 3.

To aid in the detection of diffuse structure we also imaged using a *uv*-taper of $2.5 \text{ k}\lambda$, giving an effective beam size of $\approx 60''$. The rms noise is $\approx 2 \text{ mJy beam}^{-1}$, largely due to confusion from unresolved sources in the Galactic plane; see Figure 4.

The 332 MHz data were taken at the VLA in spectral-line mode with 32 channels of 97 kHz each to aid in the excision of radio-frequency interference (RFI). We reduced the observations in **AIPS**, following the procedure for low-frequency data reduction³ (see also

²Note that STIS magnitudes are in the STMAG system, where $m = -21.1 - 2.5 \log F_{\lambda}$, with F_{λ} in units of $\text{erg s}^{-1} \text{ cm}^{-2} \text{ \AA}^{-1}$. All other magnitudes are Vega-based.

³<http://rsd-www.nrl.navy.mil/7213/lazio/tutorial/index.html>

LaRosa et al. 2000). First we removed any egregious RFI. Then we phase (using 3C 380) and gain (using 3C 286 and 3C 48) calibrated the fringe visibilities. We again searched for and removed RFI, then averaged the channels together. We mapped and self-calibrated the data iteratively, using 3-dimensional Fourier transforms in **IMAGR**, the basic AIPS deconvolution and imaging task. While imaging we used 25 planar facets arranged in a 5×5 grid, each of which had 256×256 $13''$ cells. These facets were used to mitigate the effects of non-coplanar arrays that are present at low frequencies and with wide fields (Cornwell & Perley 1992; Perley 1999). Finally, we re-assembled the facets and flattened them into a single planar map using the task **FLATN**. The rms noise is ≈ 2 mJy beam $^{-1}$, limited primarily by confusion due to unresolved emission in the Galactic plane and to sidelobes from the bright W49 complex. The final beam size is $\approx 50''$, comparable to that of the tapered 1.4-GHz images; see Figures 5 and 6.

3. Analysis & Discussion

3.1. Optical/IR

For the infrared and optical observations the astrometric uncertainty is $0''.21$. Combined with the $0''.15$ uncertainty from Frail et al. (1999), this gives us a 99% confidence radius of $0''.79$. We examined all sources in or near a circle of this radius around the position of Frail et al. (1999). In the deepest observation, the K_s -band image, we detect 7 sources that we label A–G on Figures 1 and 2. Of these, C and D are significantly blended on all the images, as are sources C and G. Sources E, F, and G are too faint to measure on the STIS image, and sources E and F are too faint to measure on the J -band image. Because of the degree of blending, we used a point-spread function (psf) fitting and subtraction technique to perform photometry on the infrared data, using the **DAOPHOT** package. First we measured the psf's of a number (≈ 30) of stars in the field without close neighbors, and constructed an average psf for each image. We then fit this psf to each source in Figures 1 and 2, subtracted the fitted stellar profile from the images, and used the subtracted images to fit the sources that were hidden by the original source. After iterating this procedure, we were able to obtain consistent magnitudes for most of the sources. For the sources that we were able to fit, all had sizes consistent with unresolved sources. For the STIS data, we adjusted the measured magnitudes to a nominal infinite aperture with a 0.13 ± 0.03 mag correction, based on the observed STIS psf⁴. We present the positions and magnitudes of sources A–G in Table 2.

⁴http://www.stsci.edu/instruments/stis/documents/ihb/stis_cy11_ihb.pdf

In Figure 7, we show a color-color diagram for the sources in Table 2 and 37 field stars for which we were able to perform reasonably accurate photometry in all bands. The sources from Table 2 all lie in the region populated by the other sources. In Figure 7 we also show model main-sequence colors (based on Cox 2000, p. 388) for $A_V = 5\text{--}10$ mag. These fit the majority of the points, with the exception of source D. However, since source D was blended with source C (making the IR photometry less reliable) and it is still in the region of the color-color diagram populated by other stars (some of whom were slightly blended themselves), we consider it unlikely that D has significantly non-stellar colors, and therefore is probably not a counterpart to SGR 1900+14 (both the disk models for AXPs [Perna, Hernquist, & Narayan 2000] and the optical/IR detection of an AXP [Hulleman et al. 2000] have non-stellar colors, and we expect something similar for SGRs). In Figure 8 we show color-magnitude diagrams for the sources in Table 2 and 37 field stars. Again, the sources populate the same region (although the field stars were chosen to be somewhat brighter than the faintest of the candidate sources), and are well bounded by model main sequences with $d = 8$ kpc and $A_V = 5\text{--}10$ mag. Source D, in particular, has slightly strange colors (also as seen in Figure 7) but its magnitudes are well within the range of the main sequence. Main sequences with $d = 12\text{--}15$ kpc and $A_V \approx 19.2$ mag, such as those plotted in Vrba et al. (2000), are too faint and too red to match these sources. Therefore the sources in Table 2 are likely to be in the foreground of the cluster found by Vrba et al. (2000).

Source G in Figures 1 and 2 and in Table 2 is too faint for accurate photometry given its proximity to other sources. It could be a counterpart of SGR 1900+14, and we require additional deep, high-resolution infrared imaging to settle this issue. Regardless, it is near our detection limit, so we can place general upper limits to the emission from SGR 1900+14 of $m_{50\text{CCD}} \gtrsim 29.0$ mag, $J \gtrsim 22.8$ mag, and $K_s \gtrsim 20.8$ mag, consistent with previously published limits (Eikenberry & Dror 2000; Vrba et al. 2000). We show these limits along with the *CXO* X-ray spectrum (Fox et al. 2001) in Figure 9. These limits translate into unabsorbed (“U”) X-ray-to-infrared flux ratios $f_X^U/(\nu_J f_{\nu,J}^U) \gtrsim 160$ and $f_X^U/(\nu_{K_s} f_{\nu,K_s}^U) \gtrsim 1.1 \times 10^3$ (assuming $A_V = 12.8$ mag). This last limit is only a factor of ~ 10 less than the detected X-ray-to- K_s limit found for the AXP 4U 0142+61 (F. Hulleman 2001, personal communication; see Figure 9) and thus we can exclude the basic disk model for AXP/SGR emission (Perna et al. 2000; see also Kaplan et al. 2001). However, if a disk does exist, then it must be truncated at $R \approx 10^{10}$ cm. As seen for SGR 0526–66 (Kaplan et al. 2001), the optical/IR limits require that the X-ray power-law break between the X-ray and the optical bands, but allow for a continuation of the X-ray blackbody.

We were able to detect but not photometer many luminous members of the massive star cluster that Vrba et al. (2000) proposed as the origin of SGR 1900+14, as we only had a small number of exposures where the central M giant stars were unsaturated. In the

remaining exposures these stars were too saturated to allow good psf subtraction, and their scattered light, bleed trails, and readout trails prevent accurate measurement of the stars in the cluster.

3.2. Radio

We do not detect either SGR 1900+14 or PSR J1907+0918 in the radio images. We therefore have 3σ limits on point source emission of 6 mJy (332 MHz) and 1.5 mJy (1.4 GHz). We also have 3σ limits on extended emission of 6.1 mJy arcmin^{-2} (332 MHz) and 6.2 mJy arcmin^{-2} (1.4 GHz).

We were able to detect SNRs G042.8+00.6, G043.3–00.2, G041.1–00.3, and possibly G043.9–01.6 at 332 MHz (Figure 5). However, G041.1–00.3, G043.3–00.2, and G043.9–01.6 are too attenuated by the primary beam of the VLA antennas for the flux measurements to be useful. For G042.8+00.6, we measure $S_{332 \text{ MHz}} = 1.24 \pm 0.08 \text{ Jy}$, excluding the contributions of point sources (see Figure 6). However, we are likely missing some flux on the shortest baselines, so this flux may be underestimated by 5%–10%.

3.2.1. Serendipitous Sources

The 332-MHz image (Figure 5) shows three sources besides the known SNRs that have shell-like morphologies but are not in the current version of the Galactic SNR catalog (Green 2000) or in any online database. We consider these sources to be candidate SNRs; with only limited data at other wavelengths we are unable to confirm an SNR classification for any of the three. The sources could be H II regions or other similar sources and require additional confirmation. Here we present what limited information we have on each.

The first source is G043.5+00.6 (see Figure 10). Its center is at position $\alpha_{2000} = 19^{\text{h}}08^{\text{m}}26^{\text{s}}$, $\delta_{2000} = +09^{\circ}42.0'$. It is circular, with radius $\approx 8.7'$. The total flux at 332 MHz is $1.05 \pm 0.08 \text{ Jy}$ (excluding the point source to the south-east), with an average surface brightness of $\approx 3.9 \text{ mJy } \text{arcmin}^{-2}$. The edge appears to be brighter, with typical surface brightness of 6–8 mJy arcmin^{-2} , while the interior is more typically 1–3 mJy arcmin^{-2} .

Without a measurement at another frequency, it is hard to determine the properties of G043.5+00.6. We were not able to find any archival X-ray or radio data at this position that could definitively classify G043.5+00.6. However, there is a marginal detection in the 1.4-GHz NRAO VLA Sky Survey (NVSS; Condon et al. 1998). The source is present in the NVSS with the same general morphology although it is too faint to measure a flux. This

faintness, though, suggests that G043.5+00.6 is not a thermal source region, as it would have a NVSS flux of ~ 1 Jy and would then be easily detectable. There are two X-ray sources from the *EXOSAT* medium-energy slew survey catalog (Reynolds et al. 1999) that lie in or near G043.5+00.6: EXMS B1906+095 and EXMS B1906+094. Both sources had been associated with the X-ray binary 4U 1907+097, which is within their $\sim 10'$ position uncertainties, but the positions of the *EXOSAT* sources are closer to G043.5+00.6 than to 4U 1907+097 (Schwartz et al. 1980).

We can estimate the distance to G043.5+00.6 very roughly using the updated Σ - D relation (Case & Bhattacharya 1998). Assuming a spectral index $\alpha = 0.5$, appropriate for many shell-type SNRs (e.g. Case & Bhattacharya 1998), we find $\Sigma_{1\text{ GHz}} = 3.8 \times 10^{-21} \text{ W m}^{-2} \text{ Hz}^{-1} \text{ ster}^{-1}$, which implies a linear diameter $D \approx 40 \text{ pc}$ and distance $d \approx 8.1 \text{ kpc}$. We note that these numbers are extremely imprecise (given both intrinsic uncertainties in the Σ - D relation and in estimates of the 1-GHz surface brightness) probably having errors approaching 100%. However, this value is consistent with G043.5+00.6 being near the tangent point of spiral arm 3 of the Taylor & Cordes (1993) electron density model.

Also intriguing are the objects in Figure 5 marked G042.0–00.1 and G041.5+00.4 (see Figure 11). These objects have morphologies that are less well-determined than that of G043.5+00.6 and are further out in the VLA primary beam, so we cannot make very useful measurements, but their shapes are suggestive of either SNRs or H II regions. G042.0–00.1 is centered at $\alpha_{2000} = 19^{\text{h}}08^{\text{m}}11^{\text{s}}$, $\delta_{2000} = +08^{\circ}00.5'$, is roughly circular with radius $4.3'$, and has a 332-MHz flux of 1.8 ± 0.4 Jy (this value has been corrected for the attenuation of the primary beam of the VLA antennas and is therefore highly uncertain). The protruding region to the south-east of G042.0–00.1 was identified as an H II region on the basis of radio recombination lines by Lockman, Pisano, & Howard (1996), but their data do not mention the rest of the complex and their angular resolution should be able to distinguish between the center of G042.0–00.1 and the smaller region. G042.0–00.1 is present in the NVSS with similar morphology to the 332-MHz image and flux $S_{\text{NVSS}} = 0.3 \pm 0.1$ Jy, suggesting a non-thermal spectrum and leading to a provisional classification as an SNR.

G041.5+00.4 is centered at $\alpha_{2000} = 19^{\text{h}}05^{\text{m}}48^{\text{s}}$, $\delta_{2000} = +07^{\circ}46.1'$. It has a complicated morphology, with a brightened rim to the north-east and a compact core to the south-west ($\alpha_{2000} = 19^{\text{h}}05^{\text{m}}37^{\text{s}}$, $\delta_{2000} = +07^{\circ}44.8'$), suggestive of a pulsar wind nebula. The source has an overall radius of $4.9'$ and a 332-MHz flux of 1 ± 1 Jy (again, this is a highly uncertain value). Comparison of the overall 332-MHz flux with the NVSS flux of 1.3 ± 0.2 Jy leads to a flat spectrum like that of an H II region, but this is provisional. We need more data to conclusively classify these objects. Further analysis of these sources is in progress.

The wealth of information available in Figure 5, concerning both already known objects

and newly discovered ones, is readily apparent. It serves to illustrate how productive low-frequency wide-field imaging of the Galactic plane with high resolution can be (e.g. LaRosa et al. 2000).

We would like to thank J. Lazio for his assistance with the low-frequency data reduction and D. Fox for useful comments. D.L.K. is supported by the Fannie and John Hertz Foundation, SRK by NSF and NASA, and MHvK by a fellowship from the Royal Netherlands Academy of Arts and Sciences. The NASA/ESA *Hubble Space Telescope* is operated by the Association of Universities for Research in Astronomy, Inc. under NASA contract No. NAS5-26555. The VLA is operated by the National Radio Astronomy Observatory, which is a facility of the National Science Foundation operated under cooperative agreement by Associated Universities, Inc. The W.M. Keck Observatory is operated as a scientific partnership among the California Institute of Technology, the University of California and the National Aeronautics and Space Administration. The Observatory was made possible by the generous financial support of the W.M. Keck Foundation. We have made extensive use of the SIMBAD database, and we would like to express our appreciation of the astronomers who maintain this database.

REFERENCES

- Bessell, M. S., Castelli, F., & Plez, B. 1998, A&A, 333, 231
- Case, G. L. & Bhattacharya, D. 1998, ApJ, 504, 761
- Chatterjee, P., Hernquist, L., & Narayan, R. 2000, ApJ, 534, 373
- Condon, J. J., Cotton, W. D., Greisen, E. W., Yin, Q. F., Perley, R. A., Taylor, G. B., & Broderick, J. J. 1998, AJ, 115, 1693
- Cornwell, T. J. & Perley, R. A. 1992, A&A, 261, 353
- Cox, A. N. 2000, Allen's astrophysical quantities, 4th edn. (AIP Press/Springer: New York)
- Deutsch, E. W. 1999, AJ, 118, 1882
- Duncan, R. C. 2001, in Proceedings of Rome Mini-Workshop on SGRs, ed. M. Feroci & S. Mereghetti (astro-ph/0106041)
- Duncan, R. C. & Thompson, C. 1992, ApJ, 392, L9

- Eikenberry, S. S. & Dror, D. H. 2000, *ApJ*, 537, 429
- Evans, W. D., Klebesadel, R. W., Laros, J. G., Cline, T. L., Desai, U. D., Teegarden, B. J., Pizzichini, G., Hurley, K., et al. 1980, *ApJ*, 237, L7
- Fox, D. W., Kaplan, D. L., Kulkarni, S. R., & Frail, D. A. 2001, *ApJ*, submitted
- Frail, D. A., Kulkarni, S. R., & Bloom, J. S. 1999, *Nature*, 398, 127
- Fruchter, A. & Mutchler, M. 1998, Space Telescope Science Institute Memo, 28 July
- Fuchs, Y., Mirabel, F., Chaty, S., Claret, A., Cesarsky, C. J., & Cesarsky, D. A. 1999, *A&A*, 350, 891
- Gaensler, B. M., Slane, P. O., Gotthelf, E. V., & Vasisht, G. 2001, *ApJ*, submitted (astro-ph/0104228)
- Green, D. A. 2000, A Catalogue of Galactic Supernova Remnants (2000 August version), Mullard Radio Astronomy Observatory, Cavendish Laboratory, Cambridge, UK (available on the World-Wide-Web at <http://www.mrao.cam.ac.uk/surveys/snrs/>)
- Hulleman, F., van Kerkwijk, M. H., & Kulkarni, S. R. 2000, *Nature*, 408, 689
- Hurley, K. 2000, in Gamma-Ray Bursts: 5th Huntsville Symposium, ed. R. M. Kippen, R. S. Mallozi, & G. J. Fishman, 763 (astro-ph/9912061)
- Hurley, K., Cline, T., Mazets, E., Barthelmy, S., Butterworth, P., Marshall, F., Palmer, D., Aptekar, R., et al. 1999a, *Nature*, 397, 41
- Hurley, K., Kouveliotou, C., Cline, T., Mazets, E., Golenetskii, S., Frederiks, D. D., & van Paradijs, J. 1999b, *ApJ*, 523, L37
- Hurley, K., Kouveliotou, C., Woods, P., Cline, T., Butterworth, P., Mazets, E., Golenetskii, S., & Fredericks, D. 1999c, *ApJ*, 510, L107
- Hurley, K., Li, P., Kouveliotou, C., Murakami, T., Ando, M., Strohmayer, T., van Paradijs, J., Vrba, F., et al. 1999d, *ApJ*, 510, L111
- Hurley, K., Li, P., Vrba, F., Luginbuhl, C., Hartmann, D., Kouveliotou, C., Meegan, C., Fishman, G., et al. 1996, *ApJ*, 463, L13
- Kaplan, D. L., Kulkarni, S. R., van Kerkwijk, M. H., Rothschild, R. E., Lingenfelter, R. L., Marsden, D., Danner, R., & Murakami, T. 2001, *ApJ*, 556, 399

- Kouveliotou, C., Strohmayer, T., Hurley, K., van Paradijs, J., Finger, M. H., Dieters, S., Woods, P., Thompson, C., et al. 1999, *ApJ*, 510, L115
- Kouveliotou, C., Tennant, A., Woods, P. M., Weisskopf, M. C., Hurley, K., Fender, R. P., Garrington, S., Patel, S. K., et al. 2001, *ApJ*, accepted (astro-ph/0107170)
- Kulkarni, S. R. & Frail, D. A. 1993, *Nature*, 365, 33
- LaRosa, T. N., Kassim, N. E., Lazio, T. J. W., & Hyman, S. D. 2000, *AJ*, 119, 207
- Lockman, F. J., Pisano, D. J., & Howard, G. J. 1996, *ApJ*, 472, 173
- Lorimer, D. R. & Xilouris, K. M. 2000, *ApJ*, 545, 385
- Marsden, D., Lingenfelter, R., Rothschild, R., & Higdon, J. 2000, in *Gamma-Ray Bursts: 5th Huntsville Symposium*, ed. R. M. Kippen, R. S. Mallozi, & G. J. Fishman, 847 (astro-ph/9912315)
- Marsden, D., Lingenfelter, R. E., Rothschild, R. E., & Higdon, J. C. 2001, *ApJ*, 550, 397
- Matthews, K. & Soifer, B. T. 1994, in *Infrared Astronomy with Arrays, The Next Generation*, ed. I. S. McLean (Dordrecht: Kluwer Academic Publisher), 239
- Mereghetti, S. 2000, in *The Neutron Star - Black Hole Connection*, ed. V. Connaughton, C. Kouveliotou, J. van Paradijs, & J. Ventura (NATO Advanced Study Institute) (astro-ph/9911252)
- Monet, D. E. A. 1998, in *The PMM USNO-A2.0 Catalog* (U.S. Naval Observatory, Washington DC)
- Oke, J. B., Cohen, J. G., Carr, M., Cromer, J., Dingizian, A., Harris, F. H., Labrecque, S., Lucinio, R., et al. 1995, *PASP*, 107, 375
- Paczynski, B. 1992, *Acta Astronomica*, 42, 145
- Perley, R. 1999, in *ASP Conf. Ser. 180: Synthesis Imaging in Radio Astronomy II*, ed. G. B. Taylor, C. L. Carilli, & R. A. Perley
- Perna, R., Hernquist, L., & Narayan, R. 2000, *ApJ*, 541, 344
- Persson, S. E., Murphy, D. C., Krzeminski, W., Roth, M., & Rieke, M. J. 1998, *AJ*, 116, 2475
- Predehl, P. & Schmitt, J. H. M. M. 1995, *A&A*, 293, 889

- Reynolds, A. P., Parmar, A. N., Hakala, P. J., Pollock, A. M. T., Williams, O. R., Peacock, A., & Taylor, B. G. 1999, *A&AS*, 134, 287
- Schwartz, D. A., Griffiths, R. E., Bowyer, S., Thorstensen, J. R., & Charles, P. A. 1980, *AJ*, 85, 549
- Taylor, J. H. & Cordes, J. M. 1993, *ApJ*, 411, 674
- Thompson, C. & Duncan, R. C. 1993, *ApJ*, 408, 194
- . 1995, *MNRAS*, 275, 255
- van Paradijs, J., Taam, R. E., & van den Heuvel, E. P. J. 1995, *A&A*, 299, L41
- Vasisht, G., Kulkarni, S. R., Frail, D. A., & Greiner, J. 1994, *ApJ*, 431, L35
- Vrba, F. J., Henden, A. A., Luginbuhl, C. B., Guetter, H. H., Hartmann, D. H., & Klose, S. 2000, *ApJ*, 533, L17
- Vrba, F. J., Luginbuhl, C. B., Hurley, K. C., Li, P., Kulkarni, S. R., van Kerkwijk, M. H., Hartmann, D. H., Campusano, L. E., et al. 1996, *ApJ*, 468, 225

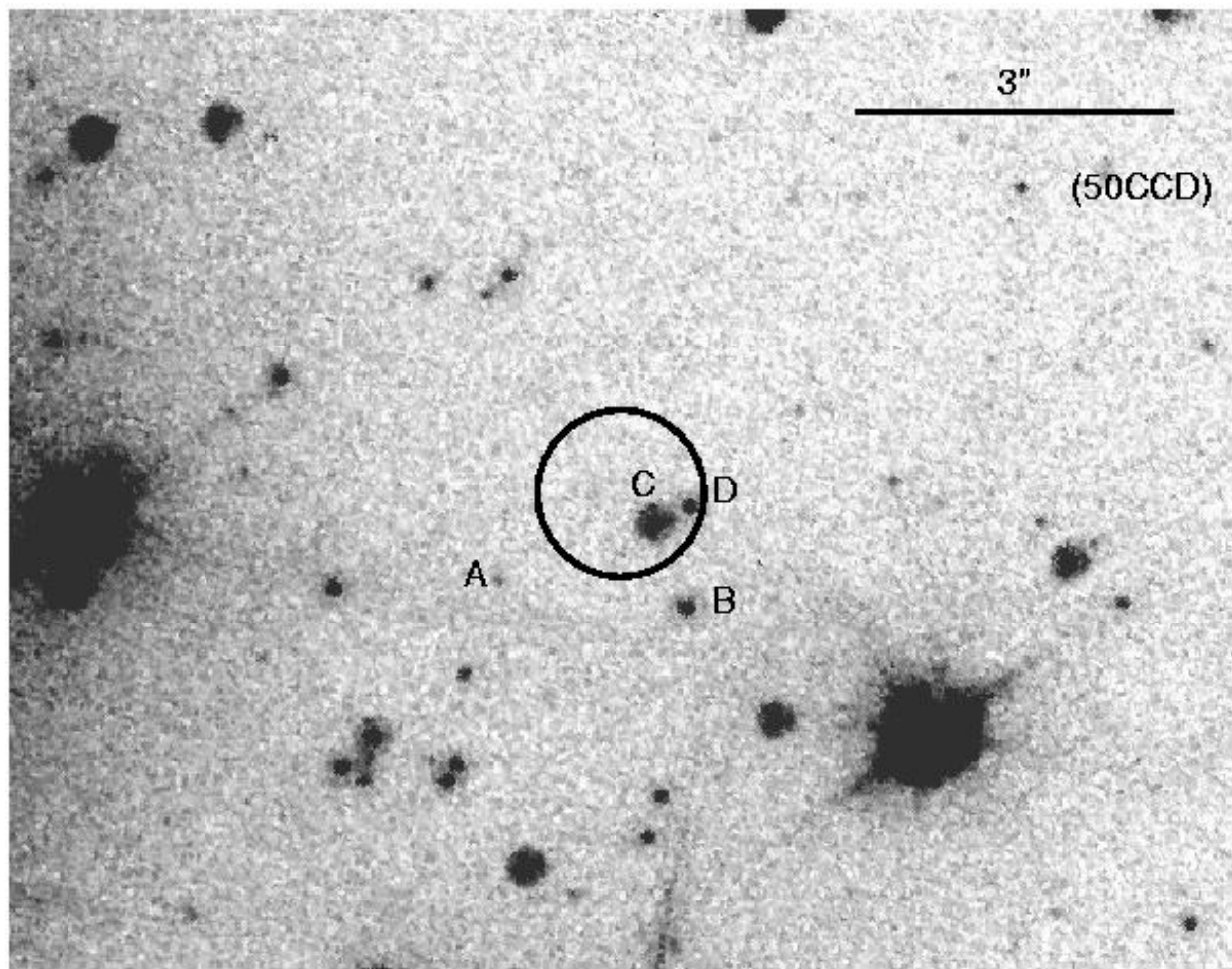


Fig. 1.— *HST/STIS* image of the region around SGR 1900+14, showing the $0''.79$ -radius error circle around the position of the transient radio source. Sources A–D are indicated. North is up, east is to the left, and the scale bar indicates $3''$. (50CCD)

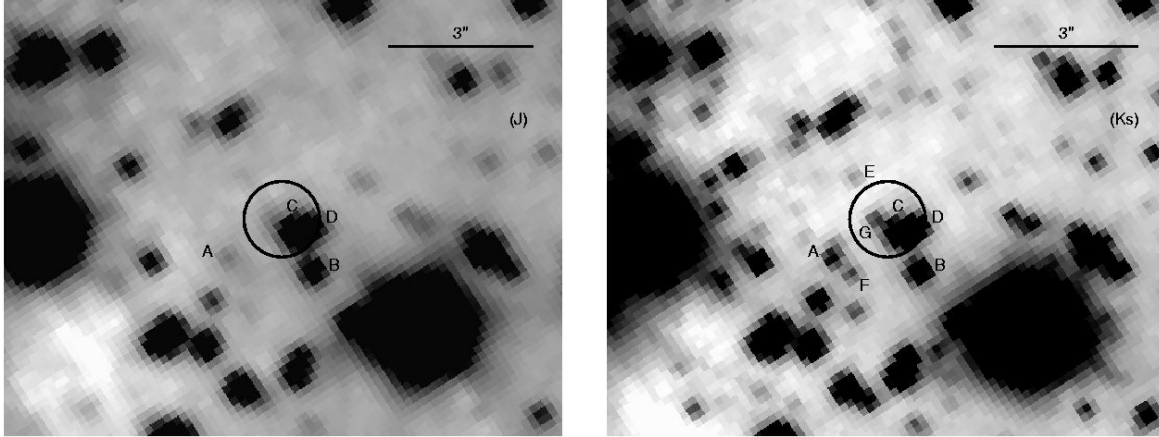


Fig. 2.— NIRC images of the region around SGR 1900+14, showing the $0.^{\prime\prime}79$ -radius error circle around the position of the transient radio source. J -band (left); K_s -band (right). Sources A–G are indicated. We were unable to perform photometry for source G in any image. North is up, east is to the left, and the scale bar indicates $3''$.

Table 1. Observation Summary

Date	Telescope / Instrument	Band	λ	Exposure (min)	Comments
1998 Sep 05	Keck I/NIRC	K_s	$2.15 \mu\text{m}$	49.7	0''.35 seeing
		J	$1.25 \mu\text{m}$	22.5	
1998 Nov 18	VLA	L	20 cm	76	D-config.
1998 Dec 26	VLA	P	90 cm	441.5	C-config., 32 channels
1999 Apr 26	VLA	L	20 cm	116	C-config.
2000 Apr 12	<i>HST</i> /STIS	50CCD	$0.585 \mu\text{m}$	86.6	

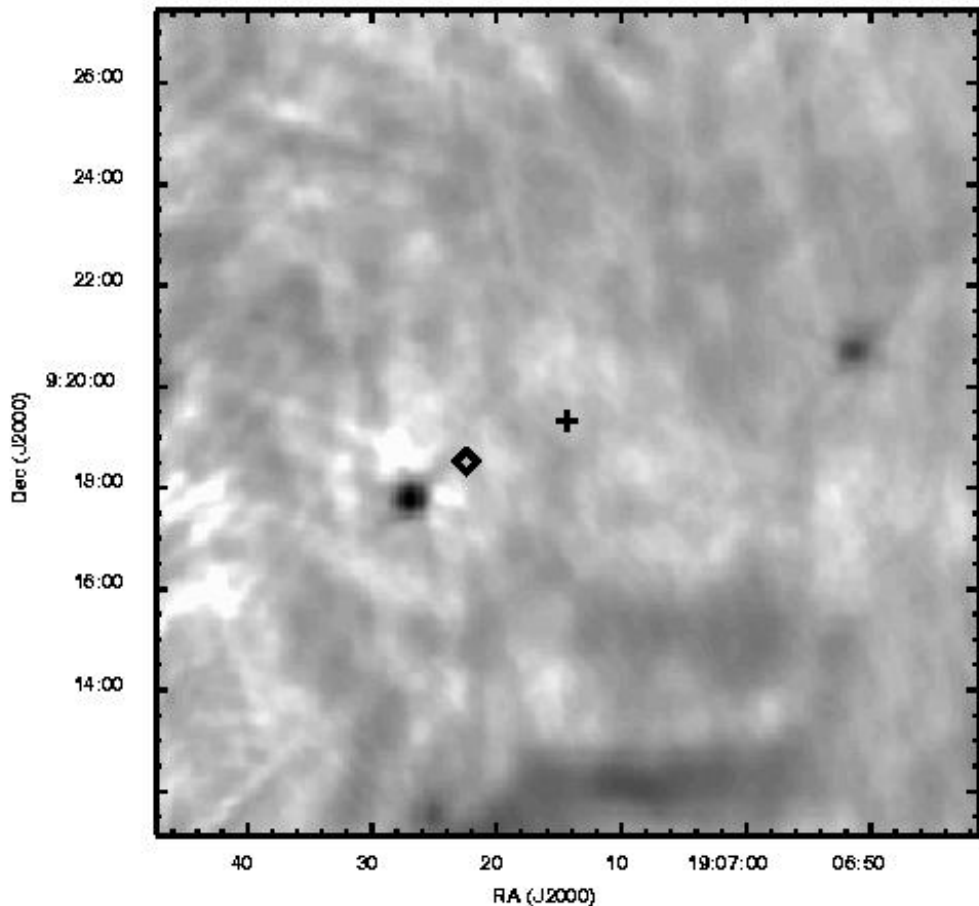


Fig. 3.— 1.4-GHz VLA image of the region around SGR 1900+14. The cross marks the position of SGR 1900+14, and the diamond marks the position of PSR J1907+0918. The northern rim of SNR G042.8+00.6 is visible. The radio source to the south-east of PSR J1907+0918 is not related.

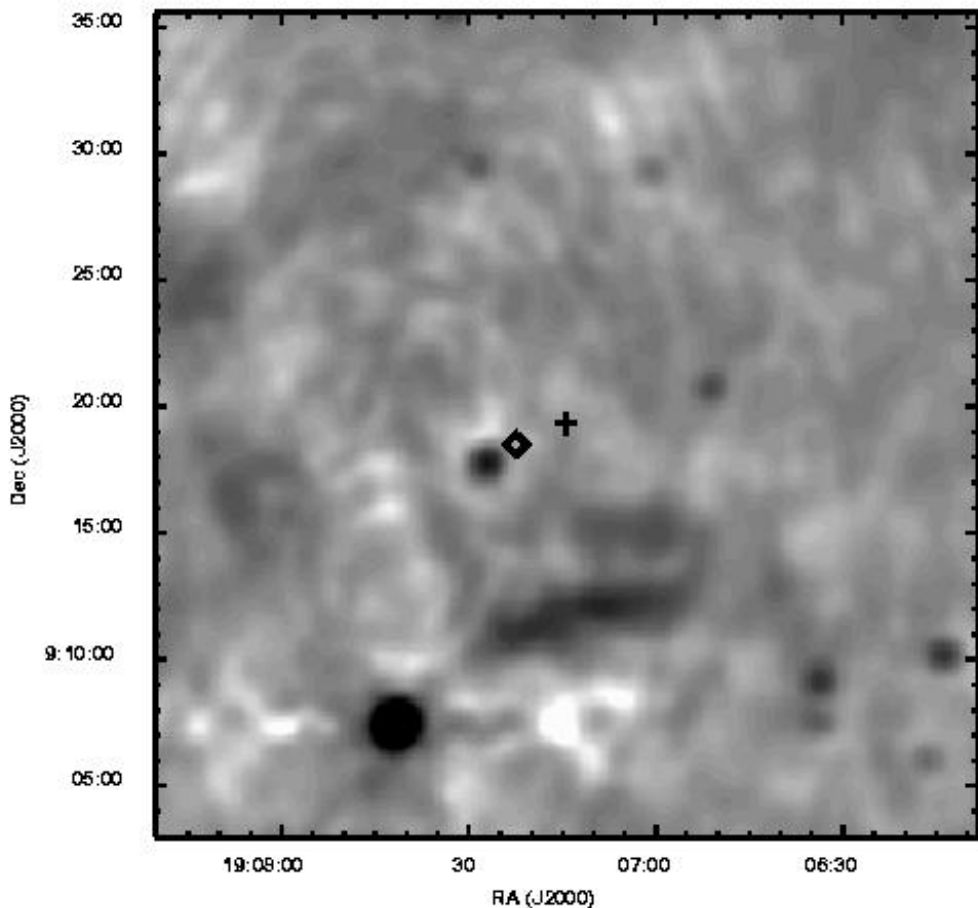


Fig. 4.— 1.4-GHz VLA image of the region around SGR 1900+14, tapered to $\sim 60''$ resolution. The cross marks the position of SGR 1900+14, and the diamond marks the position of PSR J1907+0918. The radio source to the south-east of PSR J1907+0918 is not related.

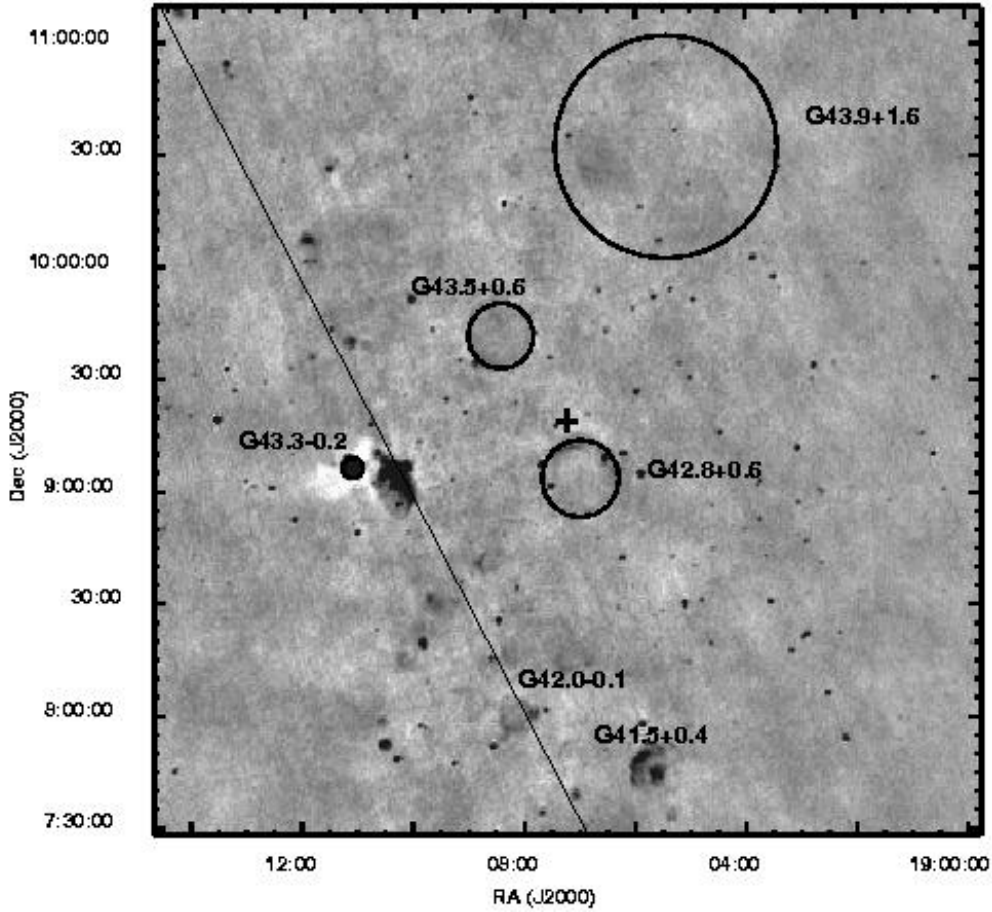


Fig. 5.— Wide-field 332-MHz VLA image of the region around SGR 1900+14. SNRs are marked by circles and/or labeled. The diagonal line is the Galactic plane. The cross marks the position of SGR 1900+14. G043.5+00.6, G042.0-00.1, and G041.5+00.4 are new candidate SNRs; see also Section 3.2.1 and Figures 10 and 11. There are a number of smaller H II regions that we have not labeled. The horizontal and vertical lines visible in some places are artifacts created when the planar facets were combined (see Section 2.3).

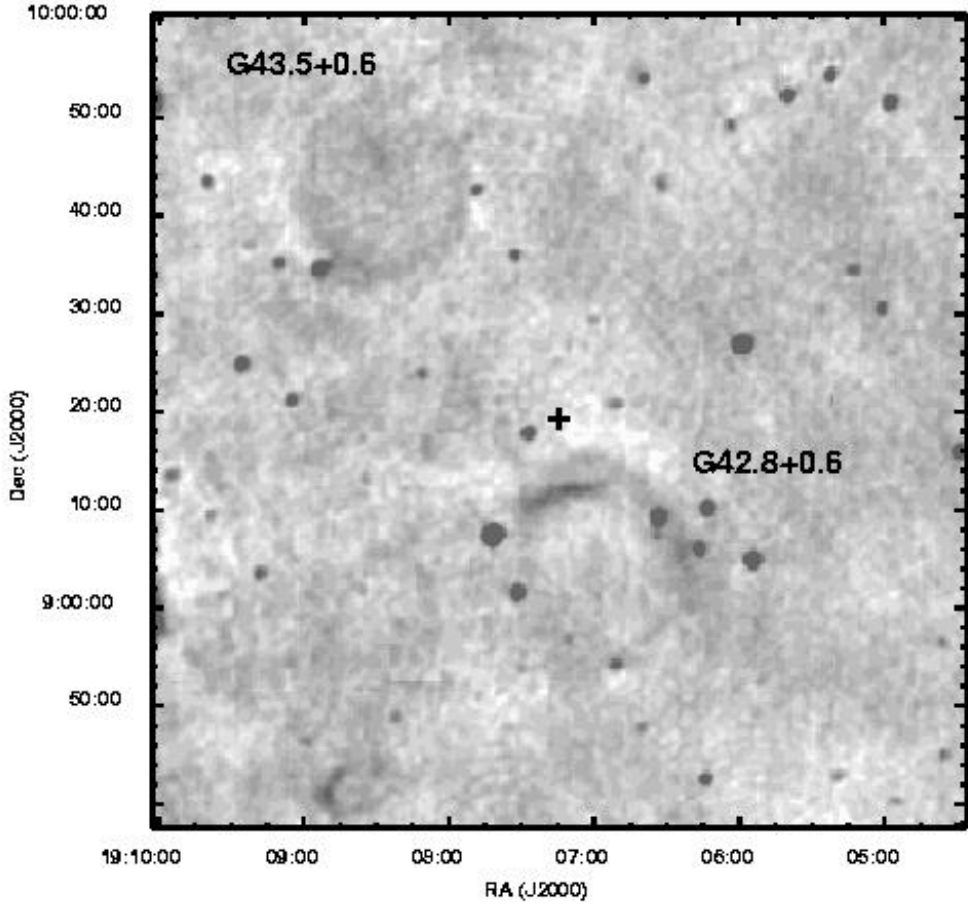


Fig. 6.— 332-MHz VLA image of the region around SGR 1900+14. SNR G042.8+00.6 and candidate SNR G043.5+00.6 are labeled. The cross marks the position of SGR 1900+14; there is no radio source at this position. The white (i.e. negative) region near SGR 1900+14 and PSR J1907+0918 is an artifact of the deconvolution process due to incomplete coverage of the uv -plane.

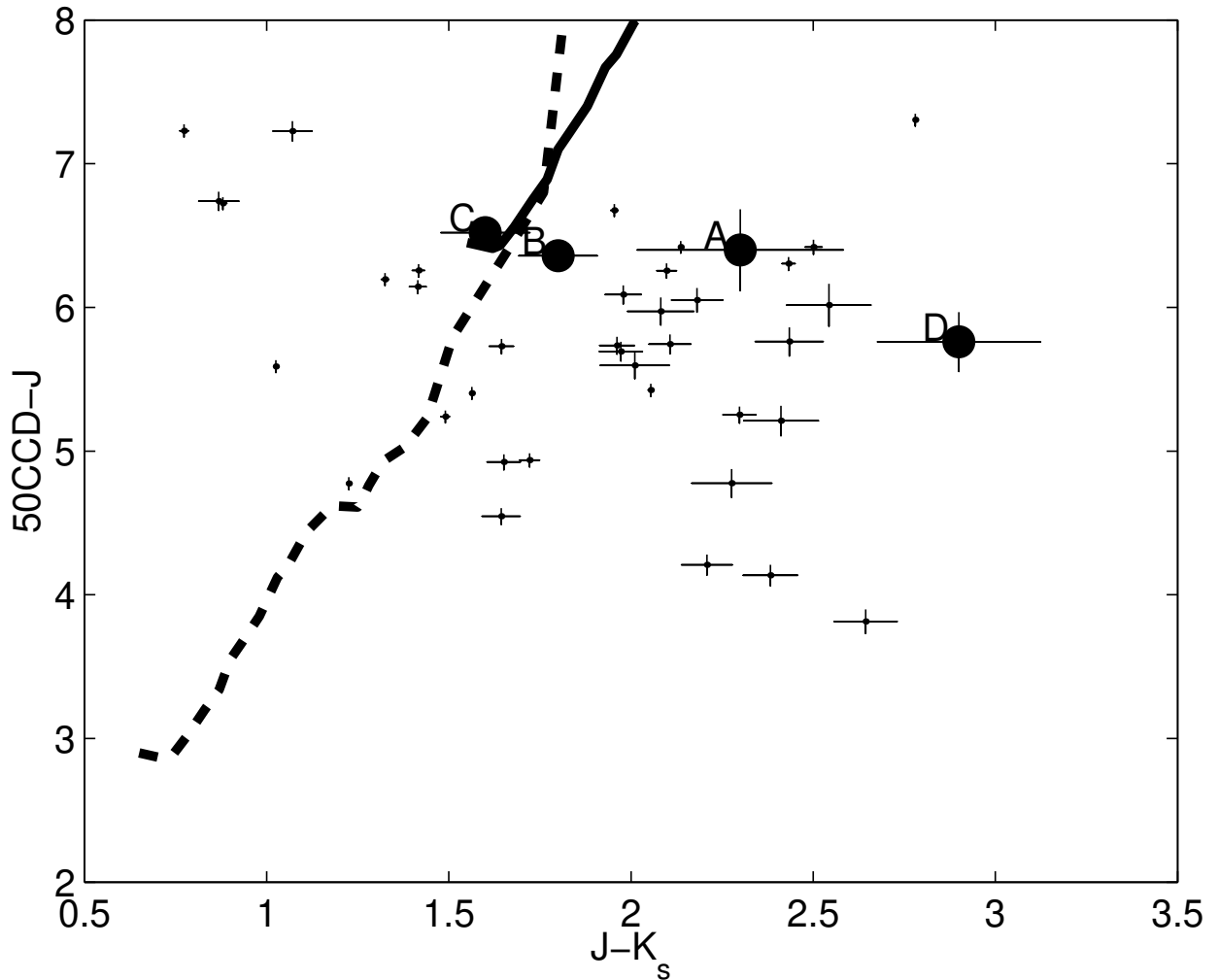


Fig. 7.— $m_{50\text{CCD}} - J$ vs. $J - K_s$ color-color diagram for the sources in Table 2 (circles) and 37 field stars (points). Also plotted are model main-sequence colors, assuming $V \approx m_{50\text{CCD}}$, for $A_V = 10$ mag (solid line) and $A_V = 5$ mag (dashed line), both at a distance of 8 kpc.

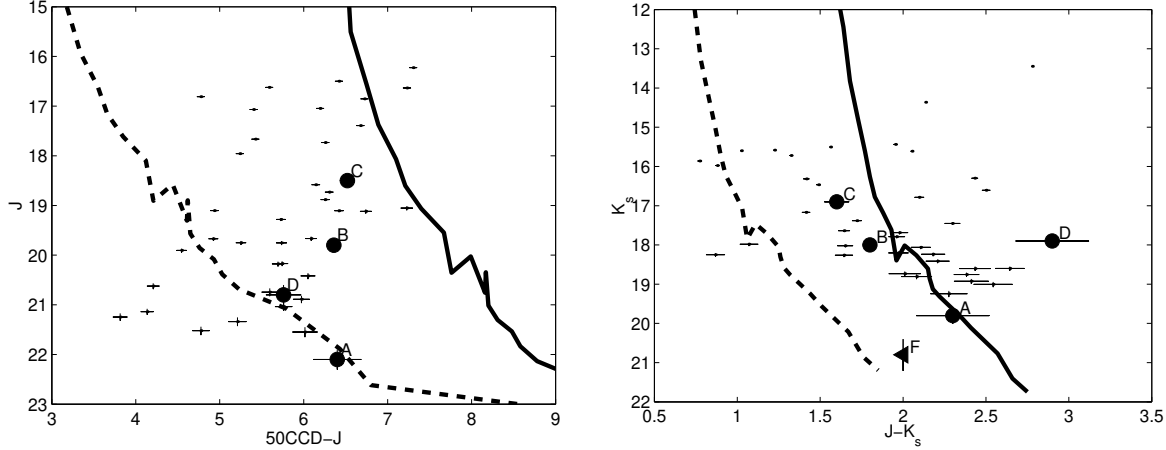


Fig. 8.— Color-magnitude diagrams for the sources in Table 2 (circles) and 37 field stars (points). Also plotted are model main-sequences, assuming for $A_V = 10$ mag (solid line) and $A_V = 5$ mag (dashed line), both at a distance of 8 kpc. J vs. $m_{50\text{CCD}} - J$ (left); K_s vs. $J - K_s$ (right).

Table 2. Stars Near SGR 1900+14 Error Circle

Label	Position ^a (J2000)		50CCD	Magnitude	
	α	δ		J	K_s
A	19 ^h 07 ^m 14 ^s .41	+09°19'19".2	28.1 ± 0.2	22.1 ± 0.2	19.8 ± 0.2
B	19 ^h 07 ^m 14.29	+09°19'19".0	26.16 ± 0.06	19.8 ± 0.04	18.0 ± 0.1
C	19 ^h 07 ^m 14.31	+09°19'19".8	25.02 ± 0.05	18.5 ± 0.07	16.9 ± 0.1
D	19 ^h 07 ^m 14.29	+09°19'20".0	26.46 ± 0.06	20.8 ± 0.2	17.9 ± 0.1
E	19 ^h 07 ^m 14.40	+09°19'22".2	> 29.0	> 22.8	20.6 ± 0.4
F	19 ^h 07 ^m 14.38	+09°19'18".9	> 29.0	> 22.8	20.8 ± 0.4
G	19 ^h 07 ^m 14.34	+09°19'20".1	> 29.0	≥ 22.8	...

Note. — See Figures 1 and 2.

^aAccurate to ±0".21.

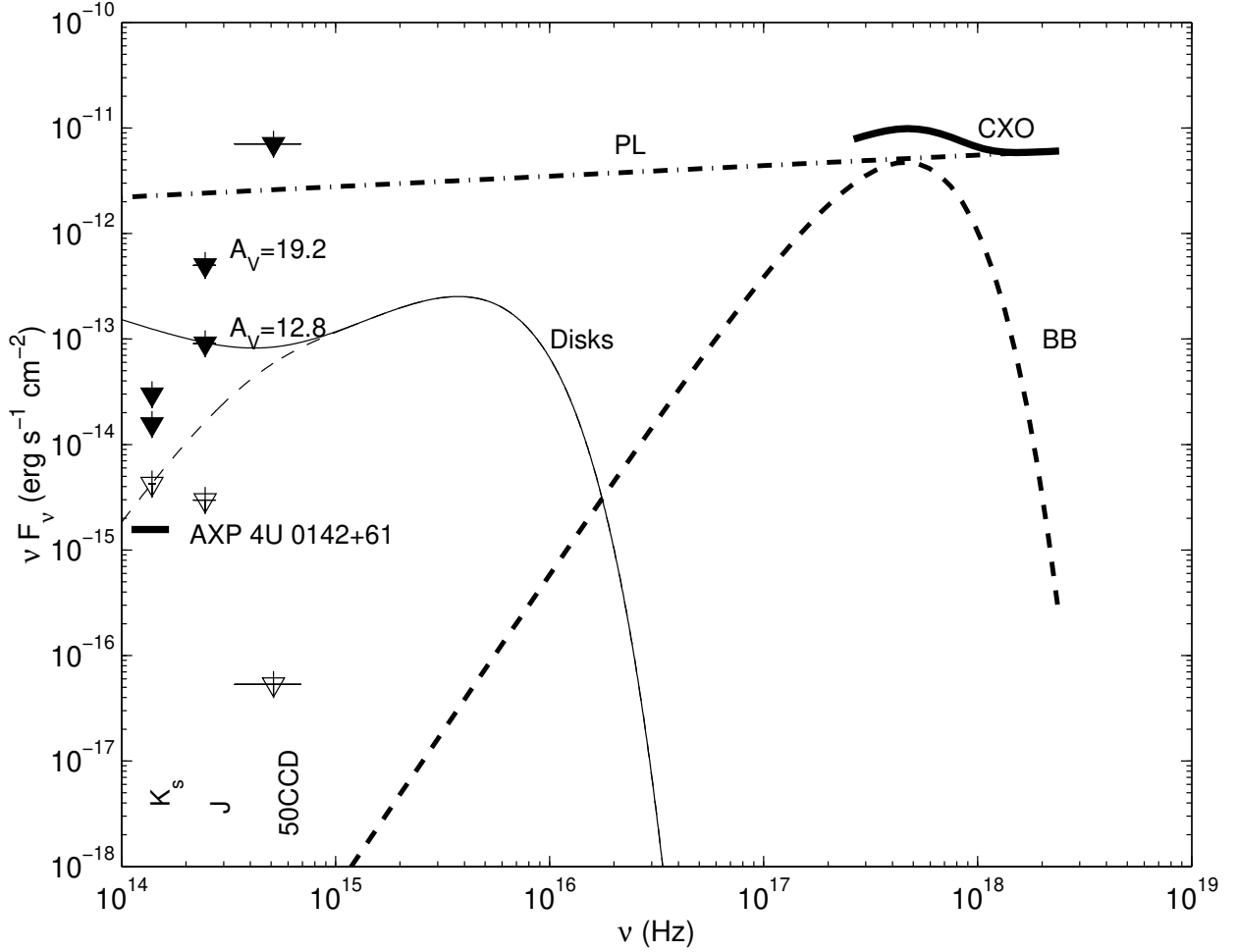


Fig. 9.— Spectral energy distribution for SGR 1900+14, including *CXO* power-law + blackbody spectrum (Fox et al. 2001; also see Hurley et al. 1999d) and upper limits. Limits are raw values (open triangles), and corrected for extinction with $A_V = 12.8$ mag and $A_V = 19.2$ mag (filled triangles). Solid thick line marked “CXO” is the measured *Chandra* spectrum; the thick dotted line marked “BB” is the blackbody component of the fit, and the thick dot-dashed line marked “PL” is the power-law component, both extrapolated to lower energies. The thick line marked “AXP 4U 0142+61” is the extinction corrected detected K_s flux of 4U 0142+61 (F. Hulleman 2001, private communication) scaled by the ratio of X-ray fluxes of 4U 0142+61 and SGR 1900+14. Also plotted are the basic disk model (thin solid line) from Perna et al. (2000), which the current limits rule out, and a disk truncated at 10^{10} cm (thin dashed line).

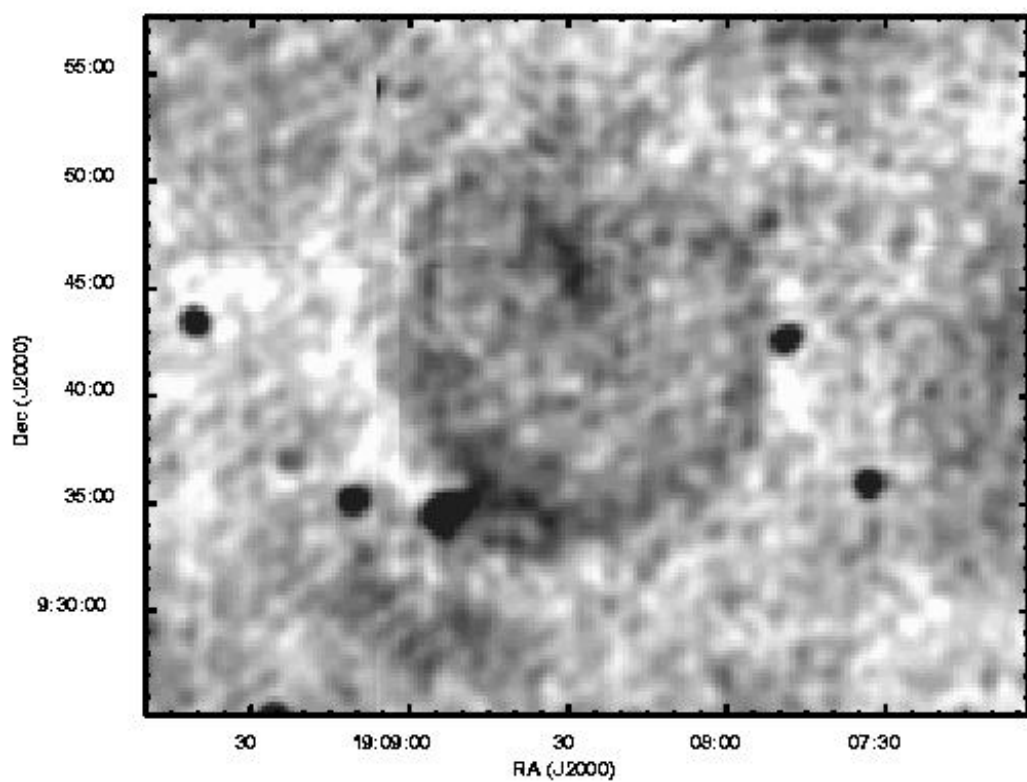


Fig. 10.— 332-MHz VLA image of candidate SNR G043.5+00.6.

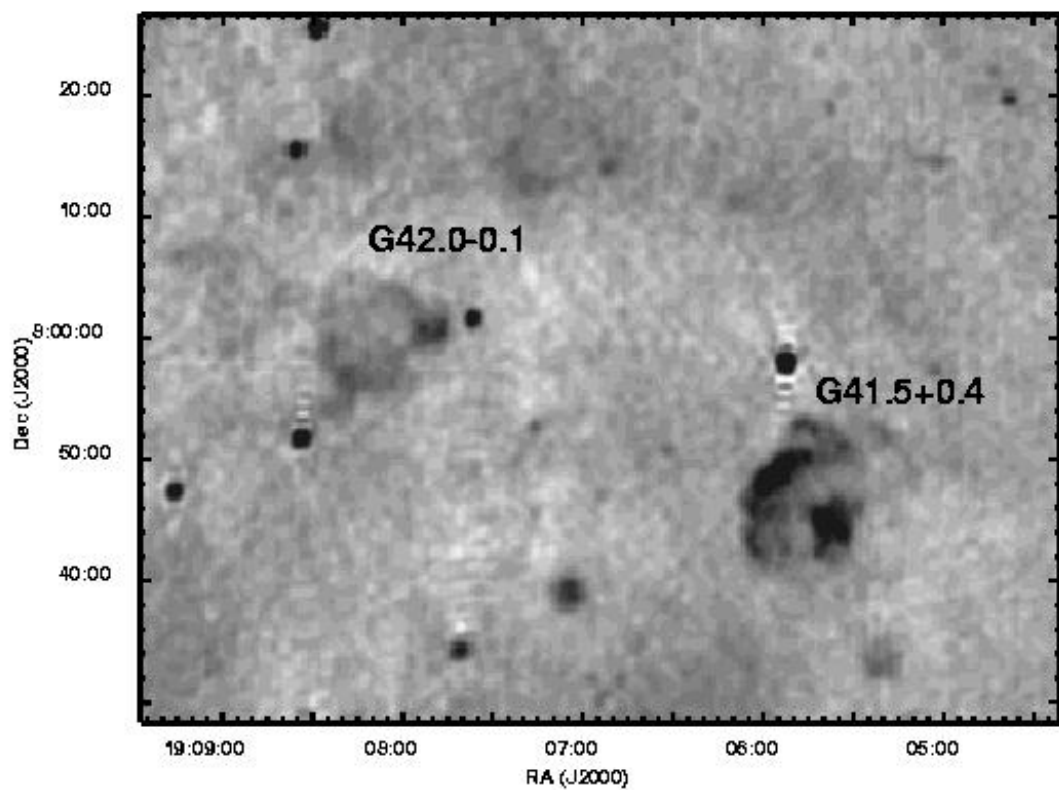


Fig. 11.— 332-MHz VLA image of candidate SNRs G042.0–00.1 and G041.5+00.4.